

Precision microwave dielectric and magnetic susceptibility measurements of correlated electronic materials using superconducting cavities

Z. Zhai, C. Kusko, N. Hakim, and S. Sridhar^{a)}

Physics Department, Northeastern University, 360 Huntington Avenue, Boston, Massachusetts 02115

A. Revcolevschi and A. Vietkine

Laboratoire de Chimie des Solides, Université Paris-Sud, 91405 Orsay, France

(Received 25 January 2000; accepted for publication 10 May 2000)

We analyze microwave cavity perturbation methods, and show that the technique is an excellent, precision method to study the dynamic magnetic and dielectric response in the GHz frequency range. Using superconducting cavities, we obtain exceptionally high precision and sensitivity for measurements of relative changes. A dynamic electromagnetic susceptibility $\tilde{\zeta}(T) = \zeta' + i\zeta''$ is introduced, which is obtained from the measured parameters: the shift of cavity resonant frequency δf and quality factor Q . We focus on the case of a spherical sample placed at the center of a cylindrical cavity resonant in the TE₀₁₁ mode. Depending on the sample characteristics, the magnetic permeability $\tilde{\mu}$, the dielectric permittivity $\tilde{\epsilon} = \epsilon' + i\epsilon''$, and the complex conductivity $\tilde{\sigma} = \sigma' + i\sigma''$ can be extracted from $\tilde{\zeta}_H$. A full spherical wave analysis of the cavity perturbation indicates that: (i) In highly insulating samples with dielectric constant $\epsilon' \sim 1$, the measured $\tilde{\zeta}_H \sim \tilde{\chi}_M$, enabling direct measurement of the magnetic susceptibility. The sensitivity of the method equals or surpasses that of dc superconducting quantum interference device measurements for the relative changes in magnetic susceptibility. (ii) For moderate $\tilde{\epsilon}$ and conductivity $\tilde{\sigma}$, $\tilde{\zeta}_H \propto \tilde{\epsilon} + i\omega\tilde{\sigma}/\epsilon_0 - 1$, thus enabling direct measurement of the sample dielectric constant $\tilde{\epsilon}$, even though the sample is placed in a microwave magnetic field. (iii) For large σ we recover the surface impedance limit. (iv) Expressions are provided for the general case of a lossy dielectric represented by $\tilde{\epsilon} + i\omega\tilde{\sigma}/\epsilon_0$. We show that an inversion procedure can be used to obtain $\tilde{\epsilon} + i\omega\tilde{\sigma}/\epsilon_0$ in a wide range of parameter values. This analysis has led to the observation of new phenomena in novel low-dimensional materials. We discuss results on magneto dynamics of the three-dimensional (3D) antiferromagnetic state of the spin chain compound Sr₂CuO₃. In dielectric susceptibility measurements in Sr₁₄Cu₂₄O₄₁, we directly observe a dielectric loss peak. Dimensional resonances in the paraelectric material SrTiO₃ are shown to occur due to the rapid increase of dielectric constant with decreasing temperature. The cavity perturbation methods are thus an extremely sensitive probe of charge and spin dynamics in electronic materials. © 2000 American Institute of Physics. [S0034-6748(00)04008-9]

I. INTRODUCTION

The continuing discovery of new electronic materials calls for new methods of measuring their electric and magnetic properties. Microwave cavity perturbation techniques have proved to be very useful for the study of transport dynamics at microwave frequencies,¹⁻⁴ in materials such as semiconductors, magnetic ferrites, and exotic materials such as charge and spin density waves (CDW, SDW).⁵

In all of these previous studies normal metal cavities were used. To study the (then) newly discovered high temperature superconductors (HTS), the use of superconducting cavities was introduced by Sridhar and Kennedy.¹ The reduction in background absorption by a factor of 10⁴ from a normal metal cavity enabled the measurement of absorption in small, single crystal superconductors and thin films. The surface impedance $\tilde{Z}_s = R_s - iX_s$ was obtained in terms of

changes of the cavity parameters: the shift in frequency δf and quality factor Q . Subsequently the concept of the ‘‘hot finger’’ technique introduced in Ref. 1 has been used in measurements in other laboratories also with the purpose of studying HTS.^{6,7}

In this article, we present a re-analysis of the cavity perturbation technique, and describe a new application utilizing superconducting microwave cavities, to study dynamic electric and magnetic susceptibilities of strongly correlated electronic materials. We focus on the configuration where the sample is placed at a microwave magnetic field maximum of the TE₀₁₁ mode.

- (1) We introduce an electromagnetic susceptibility $\tilde{\zeta} = \zeta' + i\zeta''$, which provides a useful framework to discuss the results of the microwave measurements. We use $\tilde{\zeta}_H$ to note the case where the sample is measured in a microwave magnetic field (e.g., in the TE₀₁₁ mode), and $\tilde{\zeta}_E$ when the sample is placed in a microwave electric field (e.g., in the TM₀₁₀ mode). Depending on sample proper-

^{a)}Author to whom correspondence should be addressed; electronic mail: srinivas@neu.edu

ties, the measured parameter $\tilde{\zeta}$ can be related to the sample magnetic permeability ($\tilde{\mu}=1+\tilde{\chi}_M$) and dielectric permittivity ($\tilde{\epsilon}=1+\tilde{\chi}_P$), where $\tilde{\chi}_M(\tilde{\chi}_E)$ are the magnetic (electric) susceptibilities, the conductivity $\tilde{\sigma}$, and the surface impedance Z_s . These various limits are discussed in detail in the article.

- (2) For highly insulating samples with $\tilde{\epsilon}\sim 1$, the technique is a very sensitive method of measuring the magnetic susceptibility, since $\tilde{\zeta}\sim\tilde{\chi}_M=\chi'_M+i\chi''_M$. The sensitivity of this technique is compared with others, and it is shown that the microwave method, when superconducting cavities are used, can equal or even exceed that of a dc superconducting quantum interference device (SQUID) for relative changes in susceptibility, such as with changing T . It also yields results on samples (typically mm sized) in which comparable ac susceptibility measurements do not have sufficient sensitivity. As an example of this technique we show that it yields information on magnetodynamics in a spin chain material Sr_2CuO_3 .
- (3) When the sample conductivity or dielectric constant is substantial, the measurements are dominated by these parameters. For insulating samples with even moderate dielectric constants ϵ' , the experiments are a direct measurement of $\tilde{\epsilon}=\epsilon'+i\epsilon''$. *Thus we are able to measure $\tilde{\epsilon}$ even though the sample is placed in a microwave magnetic field maximum.* (In fact, the H_ω field measurements of $\tilde{\epsilon}$ have an advantage over E_ω measurements as they are not subject to the so-called depolarization peak.) We describe an inversion procedure to obtain the complex dielectric constant $\tilde{\epsilon}+i\tilde{\sigma}/\omega\epsilon_0$ from the measured data. A spectacular example of the dielectric measurements is the observation of a dielectric loss peak in $\epsilon''(T)$ due to dielectric relaxation in the spin ladder compound $\text{Sr}_{14}\text{Ca}_{24}\text{O}_{41}$.
- (4) For sufficiently large ϵ' , dimensional resonances can occur when the microwave essentially enters into the sample. A striking example of this is presented in data on SrTiO_3 .
- (5) When the conductivity σ is appreciable, it can lead to an eddy current contribution resulting in a peak in absorption with increasing conductivity. (This is the magnetic analog of the so-called depolarization peak for E_ω field measurements.) For large conductivity the results tend to the surface impedance limit. This is the limit used in previous measurements of the surface impedance of metals and superconductors. This article presents a unified approach which encompasses both the insulating and highly metallic limits.

The cavity perturbation method discussed here yields unique information on spin and charge dynamics at short time scales between neutron scattering (NS) and nuclear magnetic resonance (NMR) and muon spin resonance (μSR), and has led to the observation of some unique phenomena in quantum magnets, dielectrics, and superconductors.

II. DESCRIPTION OF APPARATUS AND MEASUREMENT TECHNIQUE

A right cylindrical cavity (inner radius 7/8 in. and axial length 1 in.) was made of pure niobium (Nb), which is a superconductor below $T_c=8.9$ K. The cavity was fabricated in three pieces: two end plates with the needed holes and one center ring. The top plate has a center pumping hole (3.56 mm diameter), and two coupling holes (3.56 mm diameter), the bottom plate has one centrally located hole (6.7 mm diameter), through which the sample is inserted into the cavity. The TE_{011} mode is degenerate with the TM_{111} mode. As TE_{011} is the desired operating mode, the diameter of these coupling holes was chosen to provide enough perturbation to split the two modes more than 40 MHz apart. The high quality Nb stock was carefully machined at very low speed to the needed shape and then polished without lubricant, which would otherwise cause oxidation on the Nb surface. Each piece was then annealed, and the grains, which grew due to annealing, vary from sub millimeter size to roughly 4 mm diameter. The three-piece cavity was tightly held by a stainless steel assembly consisting of a top ring, a center piece for alignment, and a bottom ring. The whole resonator was then mounted in an alignment frame, supported on the top by a stainless steel Dewar probe (10.16 cm diameter and 1 m long) and, on the bottom, with a sealed copper cup (10.16 cm diameter and 10.16 cm long) with a removable bottom copper plate. Indium seals were used so that the entire assembly was vacuum tight. Superconducting operation of the cavity was accomplished using a bath of liquid ^4He .

A small piece of sample was mounted on the top of a sapphire rod (1.56 mm diameter \times 52 mm long) using very little Apiezon-N grease. The anisotropic response of the sample can be measured by mounting the sample in different orientations with respect to the applied microwave field for a given mode, as shown in the set-up diagram (Fig. 1). The sapphire rod with sample was inserted into the cavity, along its axis from the bottom, such that the sample is stationed exactly at the center of the cavity. Support and adjustment of the sapphire rod was provided by a copper tube (20 mm long), the overlap between copper tube and sapphire rod is adjustable and finally fixed with GE-varnish to guarantee good thermal contact. The copper tube was brazed at the end to a 6.35-mm-diam stainless tube (wall thickness 0.15 mm), and the stainless tube was brazed to the bottom copper plate to form a thermal path to the bottom plate which is in contact with liquid ^4He .

To heat the sample to higher temperature, a 50 Ω heating coil (0.1 mm Nichrome wire of 6.5 Ω/ft) was wound around the copper tube, and the control of the sample temperature was accomplished using an external temperature controller (Lake Shore DRC 82 C), with a silicon diode temperature sensor (Lake Shore DT 470) which is attached to the sapphire rod outside the cavity. Another temperature sensor is put in the helium chamber to monitor the bath temperature.

Microwaves were generated with a HP8510B network analyzer, a HP8341B synthesized sweeper, and a HP8513A reflection/transmission test set, and coupled into and out of the resonator from the top, through two adjustable 50 Ω co-

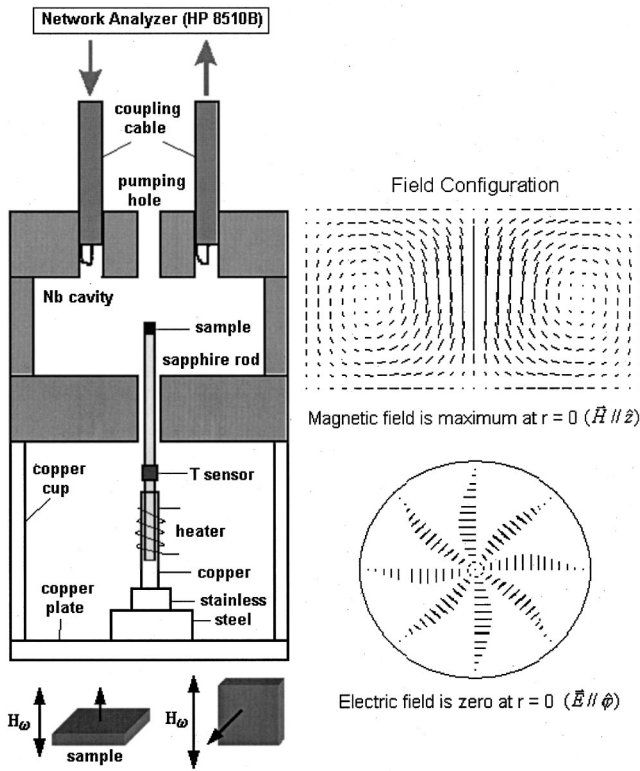


FIG. 1. (Left) Diagram for 10 GHz superconducting resonant cavity, showing the sample location and the hot finger arrangement to vary sample temperature, while keeping the cavity walls at the bath temperature. By varying sample orientation with respect to H_ω as shown, the anisotropic response can also be measured. (Right) Field configuration in the TE_{011} mode. Also shown is the (top) H_ω field lines in the (r,z) plane, and (bottom) E_ω fields at the central $(r,\theta,z=L/2)$ plane of the cavity. For this mode the sample is located at the H_ω field maximum, and at $E_\omega=0$.

axial lines, each terminated in a loop. One very useful feature of the design is the ability to vary the coupling to the resonator by moving the lines in and out along the axis of the resonator. Thus it is possible to achieve critical coupling and weak coupling over a wide range of the resonator quality factor $Q(10^4-10^8)$. For fixed coupling, input microwave power can be easily varied and the nonlinear effect of some samples can be observed.^{8,9} When operated in the TE_{011} mode the resonant cavity has the highest quality factor $Q=2 \times 10^8$ at a bath temperature of 2 K.

III. ELECTRODYNAMIC BASIS OF THE MEASUREMENT

A small sample of volume V_s placed in a resonant cavity causes the resonant frequency f and quality Q factor to change by a small amount δf . Assuming the shift in frequency is much smaller than the resonant frequency, $\delta f \ll f$, the change in cavity parameters can be expressed as^{3,10-12}

$$-\frac{\delta \tilde{f}}{f} \approx \frac{(\tilde{\mu}-1)\mu_o}{4\langle U \rangle} \int \mathbf{H} \cdot \mathbf{H}_o dV_s + \frac{(\tilde{\epsilon}-1)\epsilon_o}{4\langle U \rangle} \int \mathbf{E} \cdot \mathbf{E}_o dV_s, \quad (1)$$

where the complex frequency shift $\delta \tilde{f} = \delta f - i\Delta f/2$. Equations $\delta f \equiv f_s - f_c$ and $\Delta f \equiv \Delta f_s - \Delta f_c$ are the changes in the resonant frequency f and the resonance width Δf , respec-

tively, with (subscript s) and without (subscript c) the sample. Δf is the full width at half maximum (FWHM) of the power transmission spectrum and is related to the cavity Q factor by $\Delta f = f/Q$. $\langle U \rangle$ is the energy stored in the cavity of the resonant mode. $(\mathbf{H}_o, \mathbf{E}_o)$ and (\mathbf{H}, \mathbf{E}) are the cavity field configurations before and after the sample perturbation. A time dependence $e^{-i\omega t}$ is assumed. The terms $\tilde{\epsilon}$ and $\tilde{\mu}$ are the complex permittivity and permeability. We define the magnetic susceptibility as $\tilde{\chi}_M = \tilde{\mu} - 1 = \chi'_M + i\chi''_M$ and the dielectric susceptibility as $\tilde{\chi}_P = \tilde{\epsilon} - 1 = \chi'_P + i\chi''_P$.

It is convenient to discuss experimental results in terms of an effective dynamic or electromagnentic susceptibility ζ :

$$\delta \tilde{f} \equiv -g \tilde{\zeta} \equiv -g(\zeta' + i\zeta''), \quad (2)$$

where g is the sample geometrical factor, which is specific to the mode geometry and sample shape. Under appropriate conditions, $\tilde{\zeta}$ can be directly associated with the conventional magnetic $\tilde{\chi}_M$ or dielectric $\tilde{\chi}_P$ susceptibilities, as will be shown below.

To proceed further requires additional assumptions. Various approximations have been made, called the ‘‘quasi-static’’ (QS), ‘‘extended quasistatic’’ (EQS), and spherical wave (SW) analysis, depending on the approximation used to obtain the fields (\mathbf{H}, \mathbf{E}) . An extensive analysis was carried out by Brodwin and Parsons (BP),³ which covers essentially all the regimes needed for the experimental measurement discussed here. In the following we use BP and analyze the various regimes.

IV. SPHERICAL SAMPLE IN TE_{011} MODE

The TE_{011} configuration is well suited as a probe of the microwave response of materials because of the very high Q 's achievable in this mode. In the present experiments, the sample is located at the center of the cavity on the axis. In this location we have maximum uniform axial magnetic field \mathbf{H} and zero electric field \mathbf{E} . (See Fig. 1 for spatial profiles of the \mathbf{H} and \mathbf{E} fields). In the following we use the analysis of BP, details of which are given in the Appendix.

The geometrical factor g of a spherical sample is given as

$$g = \frac{f}{J_0^2(\beta'_{01}r_o) \left[1 + \left(\frac{\pi}{L\beta'_{01}} \right)^2 \right]} \cdot \frac{V_s}{V_c}, \quad (3)$$

where V_c is the volume of the empty cavity. $\beta'_{01}r_o$ is the first root of Bessel function $J'_0(\beta r_o) = 0$. Using the cavity inner radius $r_o = 7/8$ in., and axial length $L = 1$ in., we get $g \approx 1.036 \times 10^{15} \cdot V_s [\text{m}^{-3} \cdot \text{s}^{-1}]$, where V_s is the sample volume.

The important parameters that define the analysis are the wave vectors outside and inside the sample: $k_o = \omega/c$ and $k = k_o \sqrt{\tilde{\epsilon} + i\tilde{\sigma}/\omega \epsilon_o}$. The full-wave analysis yields in principle (see Appendix A), results for the frequency shift due to sample perturbation for a large range of sample sizes and material properties. However, in all cases of experimental interest, the sample size is much smaller than the cavity dimensions, so that the condition $k_o a \ll 1$ is rigorously satis-

TABLE I. The comparison of magnetic susceptibility measurements for microwave cavity technique and other techniques.

Method	M [$\text{A}\cdot\text{m}^2$]	Accuracy in [m^3/V_s]	χ value
Superconducting cavity	...	10^{-16} (in $f=10$ GHz)	Relative
dc SQUID	10^{-11}	10^{-16}	Absolute
ac- χ	5×10^{-10}	5×10^{-15}	Absolute
Vibrating sample magnetometer	5×10^{-8}	5×10^{-13}	Absolute
Alternating gradient force magnetometer	10^{-11}	10^{-16}	Absolute

fied. For example, if $a=1$ mm and the measuring frequency is 10 GHz, then $k_0a\approx 0.2$. In this limit, we obtain

$$\tilde{\zeta}_H = \frac{3}{2} \left(\frac{(2\tilde{\mu}+1)j_1(ka) - \sin(ka)}{(\tilde{\mu}-1)j_1(ka) + \sin(ka)} \right). \quad (4)$$

We use the subscript H to denote that the electromagnetic (EM) susceptibility $\tilde{\zeta}$ is being measured with an applied microwave magnetic field \mathbf{H}_ω .

This general form is in principle valid for arbitrary ka which is determined by material properties $\tilde{\mu}$, $\tilde{\epsilon}$, and $\tilde{\sigma}$. However, in this form it is not very useful. It is therefore necessary to consider the different limits of this expression. Below we discuss the various limits and their applicability.

A. Magnetic permeability and susceptibility measurements

More generally the result in this limit can be written as

$$\tilde{\zeta}_H = 3 \frac{\tilde{\mu}-1}{\tilde{\mu}+2} + \frac{9}{10} \left[\frac{\tilde{\mu}^2 - 6\tilde{\mu} + 4}{(\tilde{\mu}+2)^2} (k_0a)^2 + \frac{\tilde{\mu}}{(\tilde{\mu}+2)^2} (ka)^2 \right]. \quad (5)$$

Clearly the experiment measures $\tilde{\mu}$ only if the second term is negligible. This may be possible in ferromagnetic samples where $\mu' \gg 1$ provided the spins continue to respond at microwave frequencies. For weakly paramagnetic samples, we have

$$\tilde{\zeta}_H = \tilde{\chi}_M; \quad \text{where } (k_0a)^2 \tilde{\chi}_P \ll \tilde{\chi}_M. \quad (6)$$

This limit is only achieved provided the sample is highly insulating and the dielectric constant is nearly 1.

1. Sensitivity and accuracy of magnetic susceptibility measurements

Having established the relationship between magnetic susceptibility $\tilde{\chi}_M = \chi'_M + i\chi''_M$ and measured electromagnetic susceptibility $\tilde{\zeta}_H$ in Eq. (6), we can estimate the measurement sensitivity of the technique. Clearly the sensitivity is associated with both the size of samples and the cavity resonant frequency f . The bigger the sample size is, the higher the sensitivity is, as seen from Eqs. (2), (3), and (6), provided we still retain the small perturbation limit. Assuming a typical small sample has the dimension of $V_s \sim 1 \times 1 \times 0.5 \text{ mm}^3$, as in our experiment, we can detect the frequency shift δf and the absorption width Δf as small as 1 Hz in a resonant frequency of 10^{10} Hz. This results in a sensitivity limit of $\delta\zeta'_H \sim 10^{-6}$ and hence $\delta\chi'_M \sim 10^{-6}$. For comparison, Table I lists the sensitivities of some commonly

used techniques for magnetic susceptibility χ measurements.¹³ In these measurements, χ generally has the form¹³

$$\chi \approx \frac{M}{V_s H}, \quad (7)$$

where M is the magnetic moment in [$\text{A}\cdot\text{m}^2$], H is the applied magnetic field in [$\text{A}\cdot\text{m}^{-1}$]. If the same sample with volume V_s is used for all these measurements, assuming an applied field of $H \approx 10^5$ A/m corresponding to typical microwave fields, we can compare their sensitivities, as listed in Table I. Note that Eq. (6) gives the magnetic volume susceptibility $\tilde{\chi}_M = dM/dH$ in unit of Systeme International (SI) [dimensionless]. In centimeter-gram-second (c.g.s.) it is usually expressed in [$\text{emu}\cdot\text{cm}^{-3}$]. To convert from cgs to SI, a conversion multiplying factor of 4π is used.

The table shows that the hot finger cavity perturbation technique undoubtedly has one of the highest measurement sensitivities available. While other methods may require relatively large sample size and large applied field H , these are not required in the microwave measurements. However, this high sensitivity is achieved only for relative changes, such as, for instance, with varying temperature. The precision for absolute measurements is much less due to small uncertainties in sample location.

Another factor which decreases the precision of the absolute susceptibility measurements is the arbitrary shape of the sample. Throughout this article we have calculated the complex frequency shift for spherical samples only. These results can be generalized for samples with ellipsoidal geometry⁵ which in particular cases could well approximate needle-like, plate-like, and rectangular parallelepiped samples. Although the frequency shift is dependent on the shape of the measured sample, we are often interested in the variation of $\delta\tilde{f}$ with the temperature, which up to an overall geometrical constant determines with high precision the relative changes in the electric and magnetic susceptibilities.

B. Lossy dielectric, permittivity, and surface impedance measurements

For even moderate conductivity and dielectric constants, the magnetic contribution is overwhelmed by the dielectric and conductivity contributions. Taking $\tilde{\mu} \sim 1$, in the limit $\tilde{\chi}_M \ll (k_0a)^2 \tilde{\chi}_P$, we have

$$\tilde{\zeta}_H = -\frac{3}{2} \left(1 - \frac{3}{(ka)^2} + \frac{3 \cot ka}{ka} \right). \quad (8)$$

1. Dielectric permittivity and susceptibility measurements

The small ka limit of this result leads directly to a measurement of the dielectric permittivity or susceptibility

$$\begin{aligned} \tilde{\zeta}_H &\approx \frac{1}{10} (k_o a)^2 (\tilde{\epsilon} + i\tilde{\sigma}/\omega\epsilon_o - 1); \\ &\text{when } \tilde{\chi}_M \ll (k_o a)^2 \tilde{\chi}_P, \text{ and } ka \ll 1 \\ &\approx \frac{1}{10} (k_o a)^2 \tilde{\chi}_P; \\ &\text{when } \tilde{\sigma} = 0, \tilde{\chi}_M \ll (k_o a)^2 \tilde{\chi}_P, \text{ and } ka \ll 1. \end{aligned} \quad (9)$$

Therefore, in the TE_{011} mode one can measure the dielectric properties of a sample even though the sample is placed in a pure microwave magnetic field. This has nothing to do with the spatial variation of the E field near the cavity axis. It simply arises from the wave equation and holds, within geometric factors, even in a homogenous magnetic field and with zero electric field, such as can be achieved in a split ring resonator.⁶

This method of measuring $\tilde{\epsilon}$ has one important advantage over E -field cavity perturbation measurements. The measured quantity is directly proportional to $\tilde{\epsilon} - 1$ and holds even when $\tilde{\epsilon} \gg 1$ so long as $(k_o a)^2 (\tilde{\epsilon} - 1) < 1$, while in the E -field method the measured frequency shifts are proportional to $(\tilde{\epsilon} - 1)/(\tilde{\epsilon} + 2)$, due to so-called depolarization effects (see Appendix B), and can obscure the direct interpretation of the results.

For general $\tilde{\epsilon}$ Eq. (8) can be inverted to obtain $\tilde{\epsilon}$ from the measured $\tilde{\zeta}_H$. Examples of such inversions are presented later.

Note that the dielectric permittivity measured is that appropriate to the plane perpendicular to the direction of the magnetic field \mathbf{H}_ω . This is the direction of the displacement currents, and also the induced conduction currents. If the response in the plane is anisotropic then the measured $\tilde{\epsilon}$ will be an appropriate mixture of the responses in the different axes in the perpendicular plane. This must be viewed as a drawback compared to the E -field method, where in principle the response along each axis can be measured using a needle shaped specimen elongated in the direction of interest.

2. Surface impedance measurements (skin depth or eddy current limit)

The other useful limit is for a highly conducting material, where $ka = (1+i)a/\delta = (1+i)a\sqrt{\mu_o\omega\sigma}$. The skin depth $\delta = 1/\sqrt{\mu_o\sigma\omega} \ll a$, hence

$$\begin{aligned} \tilde{\zeta}_H - \zeta'_{H\infty} &= \frac{3}{\mu_o\omega a} (X_s + iR_s); \\ &\text{when } \tilde{\chi}_M \sim 0, a \gg \delta, ka \gg 1. \end{aligned} \quad (10)$$

In Eq. (10) $\tilde{\zeta}_H$ is referenced to the complete diamagnetic result $\zeta'_{H\infty} = -3/2$ for a sphere. Thus in this limit the data are a direct measure of the surface impedance

$$\tilde{Z}_s = R_s - iX_s = \sqrt{\frac{-i\omega\mu_o}{\tilde{\sigma}}}. \quad (11)$$

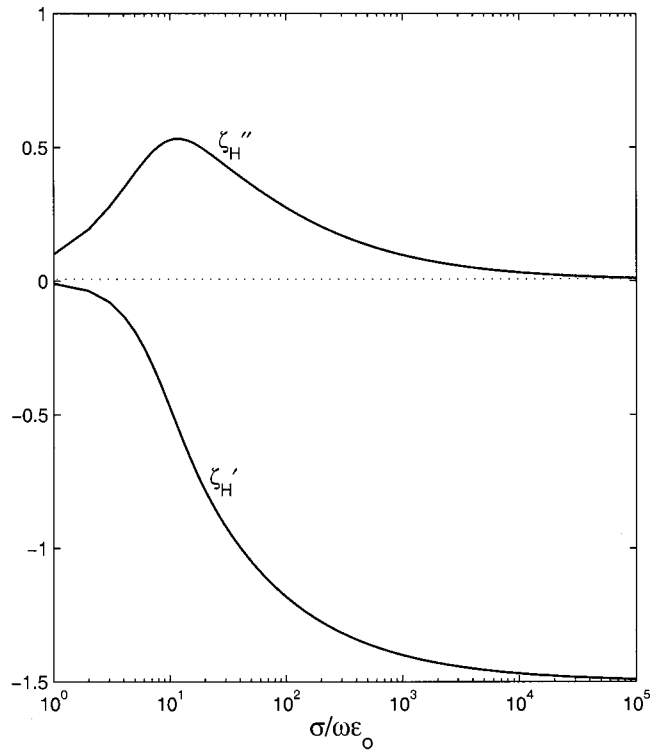


FIG. 2. The calculated dependence of the electromagnetic susceptibility ζ'_H and ζ''_H on the conductivity $\sigma/\omega\epsilon_o$. This shows the conductivity peak as σ is varied.

The normalization factor $3/(\mu_o\omega a)$ is specific to the spherical sample and TE_{011} mode geometries. Note that in this limit the measured data are $\propto 1/\sqrt{\sigma}$.

It is worth noting that this result (11) is also valid for complex conductivity $\tilde{\sigma} = \sigma_1 + i\sigma_2$ such as for a superconductor. The above treatment assumes that displacement current effects are negligible. If they are also present and can be represented in terms of a dielectric constant $\tilde{\epsilon}$, then we can also write

$$\tilde{Z}_s = R_s - iX_s = \sqrt{\frac{-i\omega\mu_o}{\tilde{\sigma} - i\omega\tilde{\epsilon}}}. \quad (12)$$

3. Conductivity (eddy current), peaks and dielectric loss peaks

As noted above, the measured changes in the cavity resonance parameters expressed here in terms of the electromagnetic susceptibility $\tilde{\zeta}_H$ change from a $\propto\sigma$ dependence for small σ to a $\propto 1/\sqrt{\sigma}$ dependence for large σ . Thus as σ is varied this results in a peak in the absorption or in ζ''_H , accompanied by a change of ζ'_H from 0 to $\zeta'_{H\infty} = -1.5$, as shown in Fig. 2. This conductivity or eddy current peak is similar to the depolarization peak observed in E -field measurements. Of course the location of the conductivity peak is determined by both the conductivity and the sample dimensions.

In certain materials, particularly the oxides, there are dielectric loss peaks intrinsic to the material, arising from a dielectric constant $\tilde{\epsilon} = \epsilon' + i\epsilon'' = \epsilon(0)/(1 + i\omega\tau)$. Usually τ is a strong function of temperature T , and hence when T is

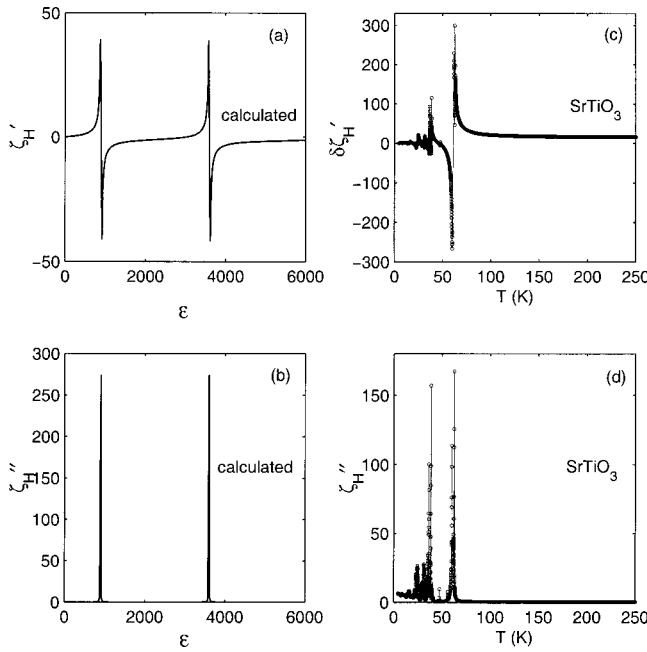


FIG. 3. (a) ζ'_H and (b) ζ''_H vs ϵ calculated using Eq. (8). The plots show the dimensional resonances which occur when $ka = (n + 1/2)\pi$. Experimental data of (c) $\delta\zeta'_H$ and (d) ζ''_H vs T for SrTiO_3 . The dimensional resonances, similar to (a) and (b), are clearly visible. In this material the dielectric constant ϵ' increases with decreasing T .

varied, a peak in $\epsilon''(T)$ occurs at a peak temperature T_p where $\omega\tau(T_p) = 1$. Since $\tau(T)$ increases with decreasing T , this peak shifts to lower peak temperatures T_p when the measurement frequency is decreased. Since $\tilde{\zeta}_H$ is proportional to $\tilde{\epsilon}$ in the appropriate limit, a peak will be observed in ζ''_H also as T is varied.

In such materials $\sigma(T)$ is also a strong function of T and typically is semiconducting: $\sigma(T) = \sigma_o \exp(-T_{s0}/T)$. Under such conditions, the experimental data will display two peaks, one a dielectric loss peak and the other a conductivity peak, as T is varied. When the measuring frequency ω is reduced, the dielectric loss peak will move to lower T while the conductivity peak will move to higher T , i.e., the peaks move apart on the T axis with decreasing ω . A specific example of a dielectric loss peak in the spin ladder material $\text{Sr}_{14}\text{Cu}_{24}\text{O}_{41}$ is discussed later.

4. Dimensional resonances

A remarkable prediction of Eq. (8) is the occurrence of dimensional resonances when the dielectric constant varies strongly. This is shown in Figs. 3(a) and 3(b). The resonances occur whenever $ka = (n + 1/2)\pi$ and are quite sharp. They correspond to situations where the electromagnetic field essentially resonates inside the sample, just like a dielectric resonator. We have observed such resonances in SrTiO_3 , which can be viewed as a quantum paraelectric with transition temperature at $T = 0$, and in which material ϵ' increases rapidly with decreasing T to values approaching several thousands. Results are discussed later.

V. EXPERIMENTAL PROCEDURES

In the experiment, we first carry out a background run to measure the resonance frequency $f_c(T)$ and the width $\Delta f_c(T)$ of the empty cavity as a function of T . Then the sample is inserted and corresponding parameters $f_s(T)$ and $\Delta f_s(T)$ are measured. $\tilde{\zeta}_H = \zeta'_H(T) + i\zeta''_H(T)$ is obtained using

$$\zeta'_H(T) = -\frac{1}{g}[f_s(T) - f_c(T)], \quad (13)$$

$$\zeta''_H(T) = \frac{1}{g}[\Delta f_s(T) - \Delta f_c(T)].$$

The term g is given by Eq. (3). In practice, while relative changes $\delta f_s(T) = f_s(T) - f_s(T_{\text{ref}})$ or $\delta f_c(T) = f_c(T) - f_c(T_{\text{ref}})$ referred to a reference temperature T_{ref} can be measured with extremely high precision, there can be larger errors in the absolute value of $f_s(T) - f_c(T)$. For this reason we represent the data as

$$\zeta'_H(T) = -\frac{1}{g}\{[\delta f_s(T) - \delta f_c(T)] + \delta f(T_{\text{ref}})\}. \quad (14)$$

In many cases, the background correction $\delta f_c(T)$ can be negligible. It is convenient to present the data as $\delta\zeta'_H(T) = \zeta'_H(T) - \zeta'_H(T_{\text{ref}})$ instead of $\zeta'_H(T)$. To get the absolute value of ζ'_H , calibration can be made by putting the sample into the cavity to measure f_s and then immediately taking the sample out to measure f_c at a fixed temperature, and thus obtain $\delta f(T_{\text{ref}})$. For many samples (e.g., see $\text{Sr}_{14}\text{Cu}_{24}\text{O}_{41}$ later), $\zeta'_H(T_{\text{ref}}) \ll \zeta'_H(T)$ particularly at high T , so that in these cases, $\delta\zeta'_H \approx \zeta'_H$.

A. Inversion of experimental $\tilde{\zeta}$ or \tilde{Z}_s data to obtain $\tilde{\epsilon}$ and $\tilde{\sigma}$

The next key step is to obtain the fundamental material property, the sample dielectric function $\tilde{\epsilon}$ or conductivity $\tilde{\sigma}$, from the experimental data represented either as $\tilde{\zeta}$ or the surface impedance \tilde{Z}_s . Two approaches are possible here:

- (1) a direct inversion of Eq. (8) for $\tilde{\zeta}(T)$ data or Eq. (11) for $\tilde{Z}_s(T)$ data to extract $\tilde{\sigma}(T) - i\omega\tilde{\epsilon}(T)$,
- (2) modeling of $\tilde{\sigma}(T) - i\omega\tilde{\epsilon}(T)$ to quantitatively match the $\tilde{\zeta}(T)$ data using Eq. (8) or $\tilde{Z}_s(T)$ data using Eq. (11).

We discuss both these procedures below.

1. Inversion of equations

We have successfully solved Eq. (8) to obtain $\tilde{z} = ka = k_o a \sqrt{\tilde{\epsilon} + i\tilde{\sigma}/\omega\epsilon_o}$ using the subroutine FSOLVE in MATLAB. The success of the solution depends crucially on the values of $\tilde{\zeta}$ or equivalently \tilde{z} . For values of ζ' , $\zeta'' \sim 1$, which is well in the QS or EQS limits, the solution is very accurate and yields the sample $\tilde{\sigma} - i\omega\tilde{\epsilon}$ with ease. In this limit $\tilde{z} \approx 1$, corresponding to typical dielectric constants $\epsilon' \leq 1000$ (for the sample and cavity sizes discussed in this article) and not too small ϵ'' . Thus for lossy dielectrics, the results for $\tilde{\epsilon}$ can be easily obtained. The results of such a solution for the material $\text{Sr}_{14}\text{Cu}_{24}\text{O}_{41}$ are discussed later in this article. Results on several other materials which have

similar properties, such as $\text{La}_{5/3}\text{Sr}_{1/3}\text{NiO}_4$, $\text{YBa}_2\text{Cu}_3\text{O}_{6.0}$, and $\text{PrBa}_2\text{Cu}_3\text{O}_{7.0}$, are described in previous and forthcoming articles.^{14,15}

Great care must be exercised in two regimes of parameter values:

- (1) When $\zeta' \gg 1$, and $\zeta'' \ll 1$, which corresponds to $ka \gg 1$ ($\epsilon' > 1000$ for the conditions of the experiments in this article). Here the resonances of $\cot(z)$ enter when $ka = (n+1)\pi/2$, leading to dimensional resonances discussed in other sections.
- (2) The metallic limit, when $\zeta' \rightarrow -1.5$, and $\zeta'' \ll 1$. In this limit it is more appropriate to use the surface impedance limit Eq. (11) rather than Eq. (8).

The principal difficulty in the above two limits is that there are many nearby minima of the underlying function, and the program quickly converges to spurious solutions. Future work will focus on this important problem.

2. Modeling the conductivity and dielectric constant to match the data

Even if the solution procedure is successful and the material $\tilde{\sigma} - i\omega\tilde{\epsilon}$ is successfully extracted, a quantitative understanding of the experimental results for $\tilde{\sigma} - i\omega\tilde{\epsilon}$ requires a model. Where the solution is not easily attained due to the difficulties mentioned above, we have found it necessary to bypass the solution procedure and instead use model calculations of $\tilde{\sigma} - i\omega\tilde{\epsilon}$ to describe the $\tilde{\zeta}$ data using Eqs. (8) and (11).

VI. EXPERIMENTAL RESULTS

We describe below measurements on three different materials all in single crystal form. These crystals have typical dimensions of $1 \times 1 \times 0.5 \text{ mm}^3$ and have been extensively characterized by a vast array of measurements: dc resistivity, dc SQUID susceptibility, x-ray diffraction (XRD), NS, and high pressure studies. Structural studies of the single crystals show that of all of these measurements indicate single phase, high quality crystals.

A. Magnetodynamics in the spin chain material Sr_2CuO_3

Sr_2CuO_3 single crystals were prepared by the floating zone technique.¹⁶ It is an insulator in a large range of temperature, and it only possesses linear Cu-O chains and is regarded as an ideal one-dimensional spin 1/2 chain. In the measurement, the sample is mounted in such a way that the microwave field $H_\omega \parallel \hat{c}$ axis. Figure 4(a) shows the plot of $\delta\zeta'_H(T) \equiv \zeta'_H(T) - \zeta'_H(2\text{K})$ vs T and $\zeta''_H(T)$ vs T for Sr_2CuO_3 . The term $\delta\zeta'_H$ shows a monotonic increase with temperature T , and ζ''_H has insignificant changes from 6 to 260 K. These results are comparable in magnitude with the dc magnetic susceptibility measurements,¹⁷ as shown in the dashed line of Fig. 4(a), and indicate that the sample perturbation effect is in the magnetic susceptibility limit $(k_o a)^2 \tilde{\chi}_P \ll \tilde{\chi}_M$, so that $\tilde{\zeta}_H \approx \tilde{\chi}_M$. Thus in this material we are essentially measuring the magnetic susceptibility.

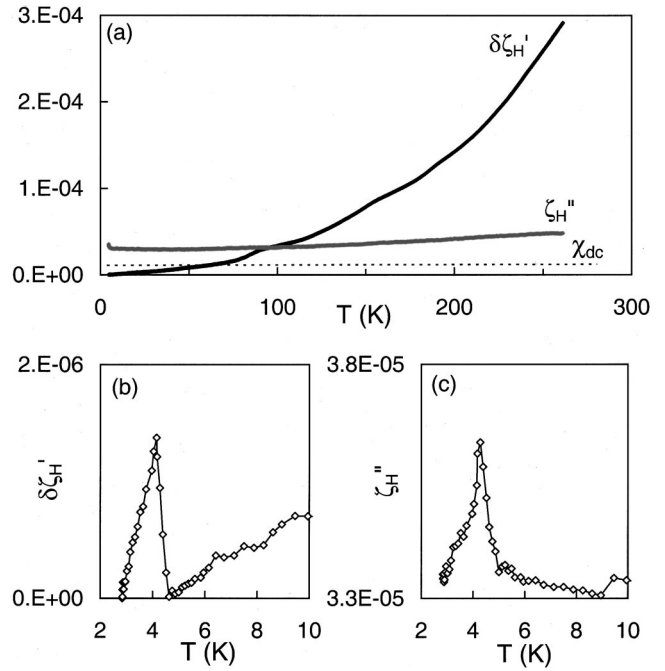


FIG. 4. (a) Measured microwave magnetic susceptibility $\tilde{\zeta}_H$ vs T for Sr_2CuO_3 . For this sample the limit $\tilde{\zeta}_H \approx \tilde{\chi}_M$ applies. Also shown is the dc susceptibility (dashed line) from Ref. 19; (b) and (c) are low T data of $\delta\zeta'_H$ and ζ''_H , showing signatures of the 3D AF transition at $T \sim 5$ K.

At low temperatures, additional features are observed in both $\delta\zeta'_H$ and $\delta\zeta''_H$, as shown in Figs. 4(b) and 4(c). These peaks are microwave signatures of the 3D long range antiferromagnetic order (AF) transition at $T_N \approx 5$ K.¹⁷ These 3D Heisenberg antiferromagnetic transitions occurring at 5 K are rather small features that have been seen only in high sensitivity dc-SQUID magnetic measurements. The very high sensitivity of the technique utilizing a superconducting cavity is evident from the similarity between the dc-SQUID and microwave data in Fig. 4.

B. Dielectric loss peaks in the spin ladder material $\text{Sr}_{14}\text{Cu}_{24}\text{O}_{41}$

There is increasing interest for studying spin/ladder compounds because superconductivity can be obtained in Ca doped $\text{Sr}_{14}\text{Cu}_{24}\text{O}_{41}$ under high pressures.¹⁸ In Fig. 5, we show the results of $\tilde{\zeta}(T)$ in the case of $H_\omega \parallel \hat{c}$ axis for $\text{Sr}_{14}\text{Cu}_{24}\text{O}_{41}$. The striking feature of the data is the rapid drop with decreasing T in $\delta\zeta''_H(T)$ below approximately 200 K, accompanied by a relatively sharp peak in $\zeta''_H(T)$ at $T \sim 170$ K, which is not seen in the dc magnetic susceptibility measurement [Fig. 5(b)]. The extraordinary dynamic range (over four orders of magnitude in $\tilde{\zeta}_H$) of the superconducting cavity enables us to see an additional peak at low T in Fig. 5(b) [the semilog plot of (a) data]. Although a similar peak is also observed in $\chi_{dc}(T)$, the magnitude is about ten times smaller than $\zeta''_H(T)$. At high temperatures, the measured $\zeta'_H/\chi_{dc} \sim 10^3$. Thus in this material the dielectric contributions dominate, i.e., $(k_o a)^2 \tilde{\chi}_P \gg \tilde{\chi}_M$, and we are thus measuring the dielectric constant.

Figure 5(c) shows the dielectric constant ϵ' and ϵ'' obtained from the measured $\tilde{\zeta}$ data and inverting Eq. (8). The

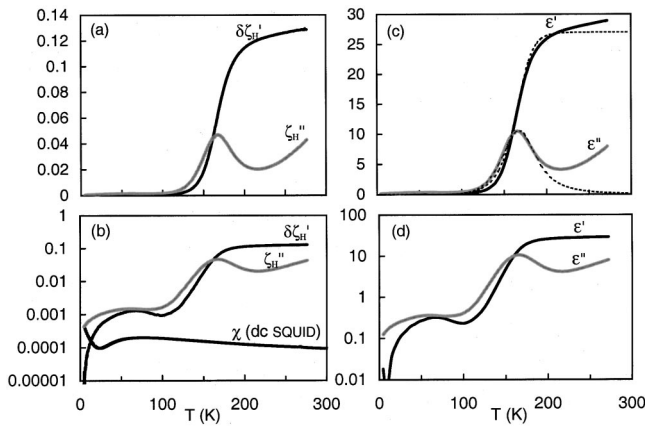


FIG. 5. Experimental data of $\delta\zeta_H'$ ($\approx\zeta_H'$) and ζ_H'' for $\text{Sr}_{14}\text{Cu}_{24}\text{O}_{41}$ in (a) linear and (b) semilog plots; (c) ϵ' and ϵ'' obtained from the ζ_H' data of (a) by solving Eq. (8). The dielectric loss peak is clearly evident. Also shown in (c) (dashed line) is the fit of the dielectric response to a Cole–Davidson form. (d) Data of (c) in a semilog plot, showing an additional feature at 110 K coincident with the opening of the magnetic gap reported in this system.

loss peak in ϵ'' is clearly evident, and is accompanied by a change of state of ϵ' . These data indicate an essentially pure dielectric relaxation process in this spin ladder material, arising from the presence of charges due to doping.

The dielectric mode is well described by a Cole–Davidson form $\tilde{\epsilon}(\omega, T) = \epsilon(0)/[1 + i\omega\tau(T)]^\beta$, with $\epsilon(0) = 27$, $\beta = 0.6$, and an activated relaxation time $\tau(T) = 1.6 \times 10^{-16} \cdot \exp(T_{\tau 0}/T)$ [s], with an activation energy $T_{\tau 0} = 2000$ K. When the relaxation rate $\tau^{-1}(T)$ varies rapidly with T and crosses the measurement frequency ω , a peak occurs at T_p , where $\omega\tau(T_p) = 1$, as shown in Fig. 5. In this material the relaxation time $\tau(T)$ appears to follow the conductivity $\sigma(T)$, indicating that the free carriers determine the polarization relaxation. Extensive details of the polarization dynamics in this material and in the related $\text{Sr}_{14-x}\text{Ca}_x\text{Cu}_{24}\text{O}_{41}$ family are discussed in a forthcoming publication.¹⁵

C. Dimensional resonances in SrTiO_3

One of the striking predictions of the above analysis is the occurrence of dimensional resonances discussed in an earlier section. These resonances occur when the dielectric constant is so large that the condition $ka = (n + 1/2)\pi$ is satisfied. We have experimentally observed such resonances in single crystal samples of SrTiO_3 measured in a TE_{011} cavity. The single crystal samples were purchased from Aesar Mfg. Co. The experimental data are shown in Figs. 3(c) and 3(d), where $\delta\zeta_H'(T)$ and $\zeta_H''(T)$ are shown as a function of T for a sample with dimensions $0.5 \times 0.5 \times 0.5$ mm³. The data clearly show resonances as a function of T . In this material ϵ' increases strongly with decreasing T approaching values of nearly 1000. The experimental data shown in Figs. 3(c) and 3(d) are quantitatively consistent with the behavior in (a) and (b).

Inversion of Eq. (8) shows a weakly T -dependent $\epsilon' \sim 850$ between 250 K and about 75 K. This value is entirely consistent with other measurements.¹⁹ However, at lower temperatures the inversion of the ζ_H' data to obtain $\tilde{\epsilon}$ is

problematical because of the dimensional resonances. Here as noted before the solutions do not appear to be unique and spurious solutions are found.

An important parameter for microwave applications is the microwave loss in SrTiO_3 . We find that $\epsilon''(T)$ varies between 0.1 and 0.25 in the temperature region between 250 K and about 75 K where smooth solutions of $\epsilon' \sim 850$ are obtained. We also note that the raw experimental data for $\tilde{\zeta}$ indicate that the biggest resonances occur at 62 K and 37 K which is exactly where dielectric anomalies have been reported in lower temperature measurements.¹⁹

D. Discussion

We have shown that a careful analysis of cavity perturbation methods, combined with the use of superconducting cavities, leads to a powerful method of measuring transport properties at microwave frequencies. The method can lead to exceptionally high sensitivities for the material properties.

A surprising result is that dielectric constants can be measured even though the sample is placed in a microwave magnetic field. One consequence of this conclusion is that many such experiments which use samples in microwave magnetic fields, such as nonresonant microwave absorption measurements,²⁰ should be carefully analyzed for the influence of dielectric properties, and not just the magnetic properties.

The resulting microwave measurements show new dynamic phenomena with time scales corresponding to the GHz frequency ranges which is not seen in static dc SQUID susceptibility measurements. The microwave measurements yield information on dynamics at time scales $\sim 10^{-11}$ s comparable to NS, but shorter than NMR and nuclear quadruple resonance (NQR) (10^{-7} s) and μSR (10^{-8} s), and are a sensitive probe of charge and spin dynamics in novel electronic materials. These results will lead us to a new perspective of how to understand other cuprates. In future publications, we will discuss the results of measurements on low-dimensional spin systems and high temperature superconductors.

ACKNOWLEDGMENTS

The authors thank R. S. Markiewicz for useful discussions. This research was supported by NSF-9711910, AFOSR-F30602-95-2-0011, ONR-N00014-00-1-0002, and NSF-INT-9726801.

APPENDIX A: SPHERICAL SAMPLE IN MAGNETIC FIELD MAXIMUM OF TE_{011} MODE

Brodwin and Parsons treated a spherical homogeneous sample with radius a in a resonant cavity when the restrictions $ka \ll 1$ and $k_o a \ll 1$ are removed. They use a method developed by Stratton²¹ in which the electric and magnetic fields inside and outside the perturbing sample are expressed as expansions of spherical vector potential functions.

The field configurations of the TE_{011} mode in cylindrical coordination $(\hat{r}, \hat{\phi}, \hat{z})$ are expressed as

$$\begin{aligned} \mathbf{H}(r, \varphi, z) = & -H_o \frac{\pi}{\beta'_{01} L} J_1(\beta'_{01} r) \cos\left(\frac{\pi z}{L}\right) \hat{r} \\ & + H_o J_0(\beta'_{01} r) \sin\left(\frac{\pi z}{L}\right) \hat{z}, \\ \mathbf{E}(r, \varphi, z) = & H_o \frac{i \omega \mu_o}{\beta'_{01}} J_1(\beta'_{01} r) \sin\left(\frac{\pi z}{L}\right) \hat{\varphi}, \end{aligned} \tag{A1}$$

where H_o is the maximum magnetic field in the center of the cavity, r_o is the radius of the cavity, L is the cavity axial length, and $\beta'_{01} r_o$ is the first root of the Bessel function $J'_0(\beta r_o) = 0$. A time dependence $e^{-i\omega t}$ is assumed in \mathbf{H} and \mathbf{E} . When a small sample with radius a is put inside the cavity, the complex frequency shift $\delta\tilde{\omega}$ for TE₀₁₁ mode is given by the following expression:³

$$\frac{\delta\tilde{\omega}}{\omega} = \frac{i9 \eta \sin^2 \alpha}{2J_0^2(\beta'_{01} r_o)} \sum_{n=1}^{\infty} \frac{2(2n+1)}{3n(n+1)} \left[\frac{P'_n(\cos \alpha)}{\sin \alpha} \right]^2 \delta_{0n} \left(\frac{a_n^r}{\rho^3} \right), \tag{A2}$$

where $\beta = \sqrt{k_o^2 - h^2} = \kappa_o \sin \alpha$, $h = \pi/L$, and $\eta = V_s/V_c$ is the filling factor. The term a_n^r is the coefficient corresponding to the reflected (scattered) field and is given by the following expression with $\rho = k_o a$ and $N\rho = ka$:

$$a_n^r = \frac{-\tilde{\mu} j_n(N\rho) [\rho j_n(\rho)]' + j_n(\rho) [N\rho j_n(N\rho)]'}{\tilde{\mu} j_n(N\rho) [\rho h_n^1(\rho)]' - h_n^1(\rho) [N\rho j_n(N\rho)]'}. \tag{A3}$$

In the following we define the sample geometrical factor γ as

$$\gamma = \frac{\eta \sin^2 \alpha}{J_0^2(\beta'_{01} r_o)}. \tag{A4}$$

$$A_1 = \frac{3\gamma}{20} \left\{ \frac{4\tilde{\mu} j_1(N\rho) - [N\rho j_1(N\rho)]'}{\tilde{\mu} j_1(N\rho) + [N\rho j_1(N\rho)]'} \right\} - \frac{3\gamma}{4} \left\{ \frac{[2\tilde{\mu} j_1(N\rho) - [N\rho j_1(N\rho)]'] \{ \tilde{\mu} j_1(N\rho) - [N\rho j_1(N\rho)]' \}}{\{ \tilde{\mu} j_1(N\rho) + [N\rho j_1(N\rho)]' \}^2} \right\}. \tag{A8}$$

1. Quasistatic limit $k_o a \ll 1$

Considering $N\rho = ka \ll 1$ the frequency shift $\delta\tilde{\omega}$ can be reduced to

$$\begin{aligned} \frac{\delta\tilde{\omega}}{\omega} = & -3\gamma \frac{\tilde{\mu} - 1}{\tilde{\mu} + 2} \\ & - \frac{9\gamma}{10} \left[\frac{\tilde{\mu}^2 - 6\tilde{\mu} + 4}{(\tilde{\mu} + 2)^2} (k_o a)^2 + \frac{\tilde{\mu}}{(\tilde{\mu} + 2)^2} (ka)^2 \right]. \end{aligned} \tag{A9}$$

If $\tilde{\mu} = 1 + \tilde{\chi}_m \approx 1$, in addition to $k_o a$, $ka \ll 1$, then the above equation reduces to

$$\frac{\delta\tilde{\omega}}{\omega} \approx -\gamma(\tilde{\mu} - 1) = -\gamma\tilde{\chi}_M = -\gamma(\chi'_M + i\chi''_M). \tag{A10}$$

Here the frequency shift $\delta\tilde{\omega}$ is a measurement of the complex magnetic susceptibility $\tilde{\chi}_M$.

Considering the cavity resonant frequency $\omega_{mnp} = c\sqrt{\beta_{mn}^2 + p^2\pi^2/L^2}$, γ for the TE₀₁₁ mode can be rewritten as

$$\gamma = \frac{\eta}{J_0^2(\beta'_{01} r_o) \left[1 + \left(\frac{\pi}{\beta'_{01} L} \right)^2 \right]}. \tag{A5}$$

This series in Eq. (A2) is rapidly convergent for samples with diameters less than $\lambda/2\pi$, therefore the leading term gives a good approximation for the frequency shift

$$\frac{\delta\tilde{\omega}}{\omega} = \frac{i9\gamma a_1^r}{2\rho^3}. \tag{A6}$$

Using the spherical Bessel functions: $j_1(\rho) = [\sin(\rho) - \rho \cos(\rho)]/\rho^2$, $h_1^{(1)}(\rho) = -e^{i\rho}(\rho + i)/\rho^2$, and $[\rho j_1(\rho)]' = -[\sin(\rho) - \rho \cos(\rho)]/\rho^2 + \sin(\rho)$, we can examine the results of $\delta\tilde{\omega}$ in various limits.

A. Extended quasistatic limit $k_o a \ll 1$

In this approximation, $j_1(\rho) = \rho/3 - \rho^3/30$, $h_1^{(1)}(\rho) = -i/\rho^2 - i/2 + \rho/3 + O(3)$, and $[\rho j_1(\rho)]' = 2\rho/3 - 2\rho^3/15$, $[\rho h_1^{(1)}(\rho)]' = i/\rho^2 - i/2 + 2\rho/3 + O(3)$, Eq. (A2), can be written as

$$\frac{\delta\tilde{\omega}}{\omega} = -\frac{3\gamma}{2} \left\{ \frac{2\tilde{\mu} j_1(N\rho) - [N\rho j_1(N\rho)]'}{\tilde{\mu} j_1(N\rho) + [N\rho j_1(N\rho)]'} \right\} + A_1 \cdot (k_o a)^2, \tag{A7}$$

where A_1 is the coefficient of the second order term of $k_o a$ and it is given by

2. Pure conductor: Eddy current or skin depth limit:

$$\tilde{\mu} = 1, \tilde{\epsilon} = 1, \tilde{\sigma} = \sigma$$

In this limit $ka = (1+i)a/\delta$, where $\delta = 1/\sqrt{\mu_o \tilde{\sigma} \omega}$ is the skin depth. Retaining the first order in the series of Eq. (A7), we obtain the complex frequency shift $\delta\tilde{\omega}$:

$$\begin{aligned} \frac{\delta\tilde{\omega}}{\omega} = & -\frac{3\gamma}{2} \left\{ \frac{2j_1(N\rho) - [N\rho j_1(N\rho)]'}{j_1(N\rho) + [N\rho j_1(N\rho)]'} \right\} \\ \approx & \frac{3\gamma}{2} \left[1 - \frac{3}{(ka)^2} + \frac{3 \cos ka}{ka} \right]. \end{aligned} \tag{A11}$$

By using $\cot(x+iy) = \sin 2x/(\cosh 2y - \cos 2x) - i \sinh 2y/(\cosh 2y - \cos 2x)$, we obtain the Landau and Lifshitz expressions

$$\begin{aligned} \operatorname{Re}\left(\frac{\delta\tilde{\omega}}{\omega}\right) &= \frac{3\gamma}{2} \left[1 - \frac{3}{2} \left(\frac{\delta}{a}\right) \left(\frac{\sinh \frac{2\delta}{a} - \sin \frac{2\delta}{a}}{\cosh \frac{2\delta}{a} - \cos \frac{2\delta}{a}} \right) \right], \\ \operatorname{Im}\left(\frac{\delta\tilde{\omega}}{\omega}\right) &= \frac{9\gamma}{4} \left(\frac{\delta}{a}\right)^2 \left[1 - \left(\frac{a}{\delta}\right) \left(\frac{\sinh \frac{2\delta}{a} + \sin \frac{2\delta}{a}}{\cosh \frac{2\delta}{a} - \cos \frac{2\delta}{a}} \right) \right]. \end{aligned} \quad (\text{A12})$$

In the low frequency limit where $\delta \gg a$ the above formulas become

$$\begin{aligned} \operatorname{Re}\left(\frac{\delta\tilde{\omega}}{\omega}\right) &= \frac{4\gamma}{105} \left(\frac{\delta}{a}\right)^4, \\ \operatorname{Im}\left(\frac{\delta\tilde{\omega}}{\omega}\right) &= \frac{\gamma}{5} \left(\frac{\delta}{a}\right)^2. \end{aligned} \quad (\text{A13})$$

In the high frequency limit where $\delta \ll a$ we obtain the expressions

$$\begin{aligned} \operatorname{Re}\left(\frac{\delta\tilde{\omega}}{\omega}\right) &= \frac{3\gamma}{2} - \frac{9\gamma}{4} \left(\frac{\delta}{a}\right), \\ \operatorname{Im}\left(\frac{\delta\tilde{\omega}}{\omega}\right) &= \frac{9\gamma}{4} \left(\frac{\delta}{a}\right). \end{aligned} \quad (\text{A14})$$

Therefore the complex frequency shift $\delta\tilde{\omega}$ could be written in terms of surface impedance $Z_s = R_s - iX_s$:

$$\frac{\delta\tilde{\omega}}{\omega} = \frac{3\gamma}{2} \left[1 - \frac{3}{\omega\mu_o a} (X_s + iR_s) \right] \quad (\text{A15})$$

with $R_s = X_s = \sqrt{\omega\mu_o/2\sigma}$.

3. Lossy dielectric: $\tilde{\mu}=1$, $\tilde{\epsilon}=\epsilon'+i\epsilon''$, $\tilde{\sigma}=\sigma$

In this case, $k^2 = (\omega/c)^2(\tilde{\epsilon} + i\tilde{\sigma}/\omega\epsilon_o)$, the frequency shift has a similar expression with the one derived for a perfect conductor but in this case the real and the imaginary part of the wave vector are not equal:

$$\frac{\delta\tilde{\omega}}{\omega} = \frac{3\gamma}{2} \left[1 - \frac{3}{(ka)^2} + \frac{3 \cot ka}{ka} \right]. \quad (\text{A16})$$

In the limit where $ka \ll 1$, the above equation can be written as

$$\begin{aligned} \frac{\delta\tilde{\omega}}{\omega} &\approx -\frac{\gamma}{10} (k_o a)^2 \left(\tilde{\epsilon} + i \frac{\tilde{\sigma}}{\omega\epsilon_o} - 1 \right) \\ &\approx -\frac{\gamma}{10} (k_o a)^2 \tilde{\chi}_p; \quad (\text{when } \tilde{\sigma}=0), \end{aligned} \quad (\text{A17})$$

where $\tilde{\chi}_p \equiv \tilde{\epsilon} - 1 = \epsilon' - 1 + i\epsilon'' = \chi'_p + i\chi''_p$. Here the frequency shift $\delta\tilde{\omega}$ is a measurement of the complex dielectric susceptibility $\tilde{\chi}_p$ when $\tilde{\sigma}=0$.

APPENDIX B: SAMPLE IN TM₁₁₀ ELECTRIC FIELD MAXIMUM

Although we have focused on the TE₀₁₁ mode, it is also possible to carry out measurements using the TM₁₁₀ mode.

For a sample placed in the cavity center at the microwave electric field maximum, the frequency shift is³

$$\frac{\delta\tilde{\omega}}{\omega} = \frac{i9\eta}{4J_1^2(\beta'_{01}r_o)} \sum_{n=1}^{\infty} \frac{2(2n+1)}{3n(n+1)} [P'_n(0)]^2 \delta_{0n} \left(\frac{b_n^r}{\rho^3} \right) \quad (\text{B1})$$

with the reflection coefficient³

$$b_n^r = \frac{-\tilde{\epsilon}j_n(N\rho)[\rho j_n(\rho)]' + j_n(\rho)[N\rho j_n(N\rho)]'}{\tilde{\epsilon}j_n(N\rho)[\rho h_n^1(\rho)]' - h_n^1(\rho)[N\rho j_n(N\rho)]'}. \quad (\text{B2})$$

The first order of Eq. (B1) becomes

$$\frac{\delta\tilde{\omega}}{\omega} = -\frac{3\gamma'}{2} \left\{ \frac{2\tilde{\epsilon}j_1(N\rho) - [N\rho j_1(N\rho)]'}{\tilde{\epsilon}j_1(N\rho) + [N\rho j_1(N\rho)]'} \right\} \quad (\text{B3})$$

with a new geometrical factor γ' given by

$$\gamma' = \frac{\eta}{2J_1^2(\kappa_{01}r_o)}, \quad (\text{B4})$$

where $\kappa_{01}r_o$ is the first root of the Bessel function $J_0(\kappa r_o) = 0$.

In the limit where $ka \ll 1$ the frequency shift becomes

$$\frac{\delta\tilde{\omega}}{\omega} = -3\gamma' \frac{\tilde{\epsilon} - 1}{\tilde{\epsilon} + 2} + O(2). \quad (\text{B5})$$

¹S. Sridhar and W. Kennedy, Rev. Sci. Instrum. **59**, 531 (1988).

²Millimeter and Submillimeter Wave Spectroscopy of Solids, edited by G. Grüner (Springer, New York, 1998).

³M. E. Brodwin and M. K. Parsons, J. Appl. Phys. **36**, 494 (1965).

⁴S. K. Khanna, E. Ehrenfreund, A. E. Garito, and A. J. Heeger, Phys. Rev. B **10**, 2205 (1974).

⁵N. P. Ong, J. Appl. Phys. **48**, 2935 (1977).

⁶D. A. Bonn, D. C. Morgan, and W. N. Hardy, Rev. Sci. Instrum. **62**, 1819 (1991).

⁷P. J. Petersan and S. M. Anlage, cond-mat/9805365 (1998).

⁸T. Jacobs, Balem A. Willemsen, and S. Sridhar, Rev. Sci. Instrum. **67**, 3757 (1996).

⁹Z. Zhai, H. Srikanth, S. Sridhar, A. Erb, E. Walker, and R. Flukiger, Physica C **282–287**, 1601 (1997).

¹⁰J. Müller, Z. Hochfr. Techn. Elektr. **54**, 157 (1939).

¹¹J. C. Slater, Rev. Mod. Phys. **18**, 441 (1946).

¹²D.-N. Peligrad, B. Nebendahl, C. Kessler, and M. Mehring, Phys. Rev. B **58**, 11652 (1998).

¹³R. B. Goldfarb, M. Lelental, and C. A. Thompson, in *Magnetic Susceptibility of Superconductors and Other Systems*, edited by R. A. Hein, T. L. Francavilla, and D. H. Liebenberg (Plenum, New York, 1991).

¹⁴N. Hakim, Z. Zhai, C. Kusko, P. V. Parimi, S.-W. Cheong, and S. Sridhar, 1999 Fall MRS Proceedings (submitted).

¹⁵Z. Zhai and S. Sridhar (to be published).

¹⁶A. Revcolevschi, A. Vietkine, and H. Moudou, Physica C **282–287**, 493 (1997).

¹⁷N. Motoyama, H. Eisaki, and S. Uchida, Phys. Rev. Lett. **76**, 3212 (1996).

¹⁸M. Uehara, T. Nagata, J. Akimitsu, H. Takahashi, N. Mori, and K. Kinoshita, J. Phys. Soc. Jpn. **65**, 2764 (1996).

¹⁹C. Ang, J. F. Scott, Z. Yu, H. Ledbetter, and J. L. Baptista, Phys. Rev. B **59**, 6661 (1999).

²⁰Microwave Studies of High Temperature Superconductors, edited by A. Narlikar (Nova, Commack, NY, 1996), Vol. 18.

²¹J. A. Stratton, *Electromagnetic Theory* (McGraw-Hill, New York, 1941).